Spectrochimica Acta Part A: Molecular and Biomolecular Spectroscopy xxx (xxxx) xxx

Contents lists available at ScienceDirect

Spectrochimica Acta Part A: Molecular and Biomolecular Spectroscopy

journal homepage: www.elsevier.com/locate/saa

Brain tumour homogenates analysed by surface-enhanced Raman spectroscopy: Discrimination among healthy and cancer cells

Aneta Aniela Kowalska [a,*], Sylwia Berus [a], Łukasz Szleszkowski [c], Agnieszka Kamińska [a], Alicja Kmiecik [b], Katarzyna Ratajczak-Wielgomas [b], Tomasz Jurek [c], Łukasz Zadka [b]

[a] Institute of Physical Chemistry Polish Academy of Sciences, Kasprzaka 44/52, 01-224 Warsaw, Poland
[b] Department of Human Morphology and Embryology, Histology and Embryology Division, Wroclaw Medical University, ul. Chalubinskiego 6a, 50-368 Wroclaw, Poland
[c] Department of Forensic Medicine, Forensic Medicine Unit, Wroclaw Medical University, ul. Mikulicza-Radeckiego 4, 50-386 Wroclaw, Poland

ARTICLE INFO

Article history:
Received 12 July 2019
Received in revised form 4 November 2019
Accepted 4 November 2019
Available online xxxx

Keywords:
Surface-enhanced Raman spectroscopy
Principal component analysis
Brain tumours

ABSTRACT

One of the biggest challenge for modern medicine is to make a discrimination among healthy and cancerous tissues. Therefore, nowadays big effort of scientist are devoted to find a new way for as fast as possible diagnosis with as much as possible accuracy in distinguishing healthy from cancerous tissues. That issues are probably the most important in the case of brain tumours, when the diagnosis time plays a great role. Herein we present the surface-enhanced Raman spectroscopy (SERS) together with the principal component analysis (PCA) used to identify the spectra of different brain specimens, healthy and tumour tissues homogenates. The presented analyses include three sets of brain tissues as control samples taken from healthy objects (one set consists of samples from four brain lobes and both hemispheres; eight samples) and the brain tumours from five patients (two Anaplastic Astrocytoma and three Glioblastoma samples). Results prove that tumour brain samples can be discriminated well from the healthy tissues by using only three main principal components, with 96% of accuracy. The largest influence onto the calculated separation is attributed to the spectral regions corresponding in SERS spectra to vibrations of the L-Tryptophan (1450, 1278 cm^{-1}), protein (1300 cm^{-1}), phenylalanine and Amide-I (1005, 1654 cm^{-1}). Therefore, the presented method may open the way for the probable application as a very fast diagnosis tool alternative for conventionally used histopathology or even more as an intraoperative diagnostic tool during brain tumour surgery.

1. Introduction

The largest group of primary brain tumours are astrocytic gliomas. Those tumours with higher malignancy grade are characterized by high genetic diversity and high biological aggressiveness [1]. Brain tumours, particularly high-grade (Anaplastic Astrocytoma and Glioblastoma), have poor prognosis and patient survival. The most malignant glial tumour is Glioblastoma, which accounts for over 65% of all primary brain tumours. While Anaplastic Astrocytoma give 54% of the 5-year relative survival rate in the United State after patients treatments, in the youngest patients group, the Glioblastoma, regardless of the standard treatment give only 19% of the 5-year survival rate [2]. Both subtypes of malignant gliomas may develop de novo as primary tumours, or develop as a result of progression from tumours with a lower grade of histological malignancy, as secondary tumours. [3,4] Therefore, the cancer fast diagnosis is main advantage in diseases prognosis and patient survival and it still remains the challenging task from the purely human but also economical point of view. Brain tumours are classified usually by the neuropathological evaluation dependent on molecular genetic tests, prediction of biological behaviour and patient management. Commonly used in pathology laboratories techniques include immunohistochemical staining, direct sequencing, fluorescence in situ hybridization, chromosomal genomic hybridization, and next-generation sequencing. Nowadays, in the treatment of the brain tumour, there are no preoperative or intraoperative technology to identify all tumour cells among the healthy cells. Thus, because the cancerous cells are often impossible to distinguish from normal tissue often the residual invasive cancer cells frequently remain after surgery. Recently Raman spectroscopy has been used as an intraoperative differentiation tool with a sensitivity of 93% and a specificity of 91% [5]. It also has been presented a possibility to use coherent anti-Stokes Raman scattering for brain cancer diagnosis. [6] On the other hand, the stimulated Raman scattering Microscopy can be used for biomedical imaging as an alternative to histopathology technique. [7,8] However, presented in the literature Raman based Microscopies [9,10] have some limitations, and moreover, some of them are largely influence the obtained results. For example, before using Raman-guided biopsy both, a great number of patients and the collected

* Corresponding author.
E-mail address: akowalska@ichf.edu.pl (A.A. Kowalska).

https://doi.org/10.1016/j.saa.2019.117769
1386-1425/

spectra are necessary, due to large variability of obtained spectra, which affect the outcome (the differentiation recognition). Additionally to increase the signal to noise ratio the longer integration time is necessary. However longer integration times can limit the clinical practicality of those techniques, which needs to be real-time in order to minimize disruption to the neurosurgical workflow. Last but not the least more studies involving in vivo technique are needed. Almost all these limitation surface-enhanced Raman scattering (SERS) of homogenate samples overcome. Homogenates can be prepared from the tissues normally taken out during surgery operation – in this sense a number of patients and spectra can be checked, but also differences between the spectra, coming from the various cancers, not only from the individuals, can be highlighted and studied.

Therefore, herein the surface-enhanced Raman scattering (SERS) technique combined with principal component analysis (PCA), is proposed as a useful financially and practically by rapidly replacing time-consuming and labour-intensive conventional methods since any molecular genetic abnormalities will be diagnosed various brain tumours at one single shot. SERS is an optical spectroscopy method with higher sensitivity and chemical specificity than that in conventional Raman spectroscopy. [11] The presented method is therefore competitive to presented already the coherent anti-Stokes Raman or the stimulated Raman scattering Microscopy. The phenomenon of SERS is explained by the combination of an electromagnetic (EM) mechanism and a chemical mechanism related to charge transfer (CT) between a substrate and an adsorbed molecule [12,13]. Theoretically, the electromagnetic enhancement can reach factors of 10^3–10^{11}, whilst for the chemical enhancement factors up to 10^3 were calculated [14–16]. Due to such tremendously enhancement of the Raman signals, even single molecules can be detected by SERS spectroscopy. SERS is powerful in studying nucleic acids and proteins [17], therapeutic agents [18], drugs and trace materials [19], microorganisms [20] and cells. [21] The most notable recent advances in Raman and SERS include innovative applications as bimolecular sensors for clinical diagnosis of various diseases, such as Alzheimer's or Parkinson's [22], various cancer diseases such as gastrointestinal [23–26], skin [27–31], breast [32–35], lung [36,37] and also brain [38–41].

Through this work, to transform the high-complexity SERS data into a new coordinate principal components (PCs), the principal component analysis (PCA) were performed over the recorded data [42–46]. Value of PCA in especially hyperspectral mapping, characterization, detection, identification and distribution approaches [47–52]. Based on the SERS data a fast and label-free method of differentiation between the brain tumours and healthy, control cells is presented. The reported results indicate that fast, multivariate evaluation of the multiple probes is feasible and may allow for wide application in the field of accurate cancer diagnosis, risk classification, and development of therapeutic strategies.

2. Experimental section

2.1. Tissue samples ethical approval

The study was approved by the Bioethical Committee (opinion number 665/2017) located at Wroclaw Medical University.

2.1.1. Tissues sample selection and preparation

Tissue materials - archival material in the form of tissue fragments stored at the deep-freezing temperature of selected brain tumours with Anaplastic Astrocytoma and Glioblastoma histopathological types was used for the study. Histopathological diagnosis of the brain tumour

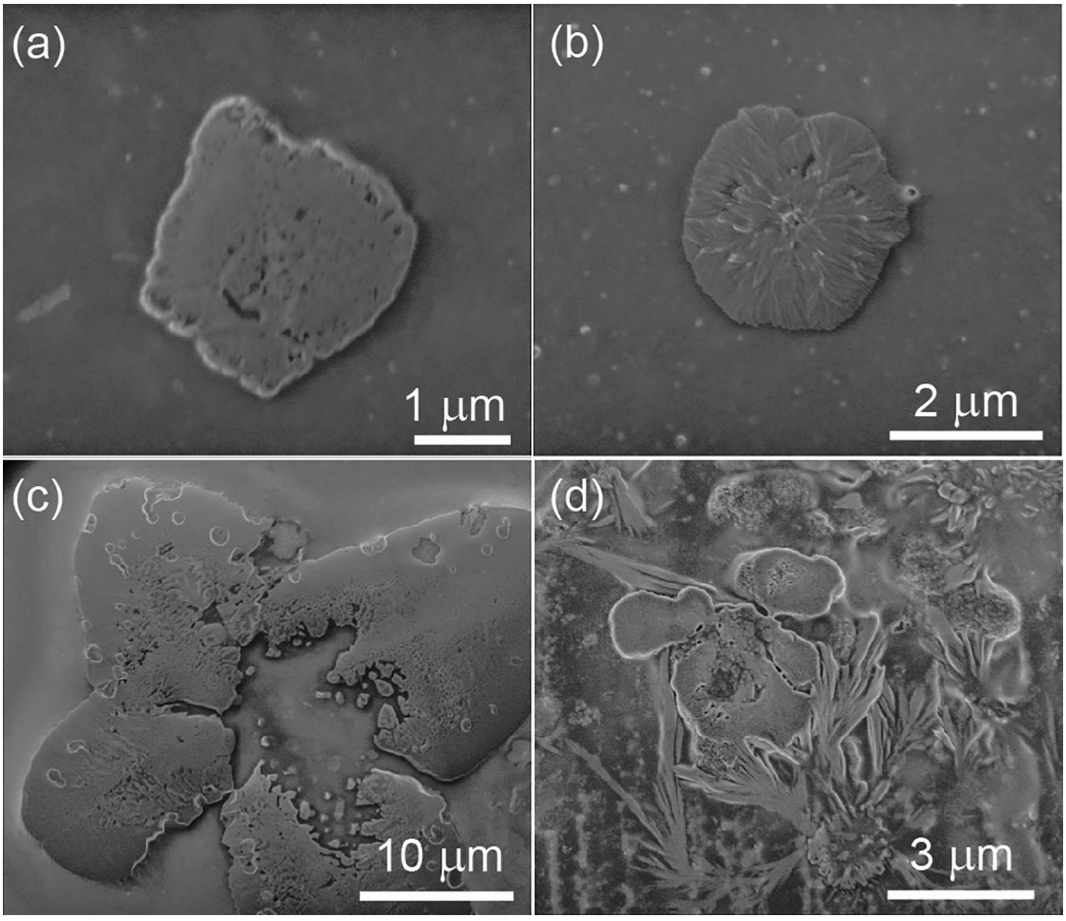

Fig. 1. SEM microscopic images of control brain tissues homogenates of temporal lobe (a,b) and gliomas brain tumour homogenates: Anaplastic Astrocytoma (c) and Glioblastoma (d).

has been confirmed by a qualified neuropathologist after surgical resection of the brain tumour. As a control, fragments of a healthy brain tissue were used. They were collected during autopsy in the Department of Forensic Medicine in Wroclaw, Poland. Exclusion criteria were as follows: tumour, intoxication and long-lasting decomposition.

Tissue homogenates - frozen material from brain tumours (two samples of Anaplastic Astrocytoma and three of the Glioblastoma, taken from five patients) and normal control (samples taken from different brain lobes of five individuals; total 40 samples) was prepared for further study with the same protocol. Tissue fragments were placed in RIPA lysis buffer: 50 mM Tris-HCl, 150 mM NaCl, 0.1% SDS, 1% IGEPAL Ca-630 and 0.5% sodium deoxycholate, pH 8.0. The prepared buffer contained 1 mM phenylmethylsulfonic fluoride (PMSF) and 0.5 μl of inhibitor cocktail (Pierce). The solution was incubated on ice for 15 min. Next, the prepared samples were centrifuged at 12000 ×*g* for 15 min at 4 °C. The supernatant was collected to Eppendorf type tubes and centrifuged again under the above-mentioned conditions. After centrifugation, the supernatant was collected into a new tube and stored at −20 °C.

2.2. Morphological characterization

The surface of prepared SERS platform were freshly dropped with studied tissue samples and then were morphologically characterized using Scanning Electron Microscope (SEM) images taken with a FEI Nova NanoSEM 450 SEM system.

2.3. Surface-enhanced Raman spectroscopy (SERS)

SERS measurements were performed using the Renishaw inVia Raman system equipped with a 300 mW diode laser emitting a 785 nm line which was used as an excitation source. The laser light was passed through a line filter and focused on a sample mounted on an XYZ translation stage with a 50× objective lens (numerical aperture 0.75) that focused the laser to a spot size of around 2.5 μm. The Raman-scattered light was collected by the same objective through a holographic notch filter to block the Rayleigh scattering. A 1200 grooves per mm grating was used to provide a spectral resolution of 5 cm^{-1}. The Raman scattering signal was recorded by a 1024 × 256 pixel RenCam CCD detector. Typically, 40 SERS spectra of control samples of each lobes from both hemispheres (20 SERS spectra for one hemisphere) and 40 SERS spectra of tumours samples were acquired for 60 s, with 8 mW of the laser power measured at the sample using mapping mode (10 μm × 10 μm) with the step size 2.6 (for 40 spectra) and 4 (for 20 spectra). The mapping measurements took approximately 30 min. Based onto recorded SERS data within one sample the average SERS spectra were calculated and presented in the manuscript.

SERS platform preparations - platforms for SERS analysis were prepared according to already published procedure [53]. Briefly, photovoltaic cells sample were cleaned with acetone and isopropyl alcohol and every each step sonificated at 50 °C by 10 min. The cleaned platforms were then dried for 30 min at 50 °C and using Physical Vapor Deposition (PVD) device the layer of silver was sputtered over SERS platforms. Such freshly prepared SERS platforms (5 × 5 mm) were used throughout presented SERS experiments. Before measurement prepared SERS platform was covered by approximately 5 μl of homogenate and let it to dry at room temperature.

2.4. Data analysis

The obtained SERS spectra were smoothed with Savitsky-Golay filter, the background was removed using baseline correction (10 itenary and 64 points), and then the spectra were normalized using a so-called Min-Max normalization (band at 677 cm^{-1} for Control and 674 cm^{-1} for tumour samples) using a built-in OPUS software package (Bruker Optic GmbH 2012 version). Then, the principal component analysis (PCA) was applied (Unscrambler, CAMO software AS, version 10.3, Norway).

3. Results and discussion

Control brain cells were acquired post mortem from patients considered healthy - with no brain injury. Five sets of control brain tissues (samples from five different individuals) from both right and left hemispheres of each lobes parts (frontal, parietal, temporal and occipital)

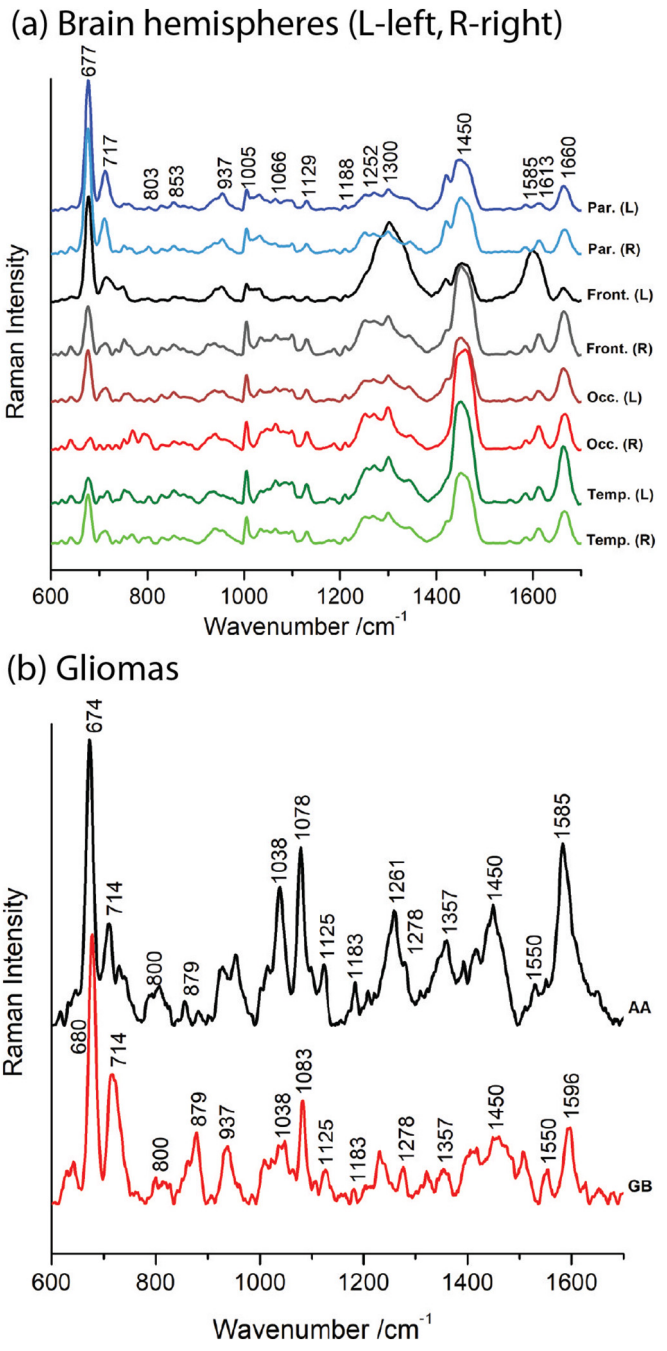

Fig. 2. The averages SERS spectra of the homogenates taken for **Control 1** from four lobes of both **L**-left and **R**-right hemispheres (a) and gliomas (b). The SERS spectra are abbreviated as **Front.**, **Par.**, **Temp.**, **Occ.** for samples taken from the frontal, parietal, temporal and occipital lobe, respectively. **AA** stands for Anaplastic Astrocytoma and **GB** for Glioblastoma spectra of the gliomas samples. SERS spectra taken in mapping mode over the platform, acquired above 20 spectra for one control sample and 40 spectra for tumour cells (160 spectra for control set which give a total 1000 spectra for controls and 200 spectra for glioma samples).

were collected and studied in order to ensure proper statistical power, in accordance to common best practice. Thus each set consists of four tissue groups from the parts of the brain, responsible for the various functions of the body. Two sets of samples that show some anomaly in their spectral features were discarded. However, three sets of brain tissues named as **1**, **2** and **3** (eight control samples from each of the three individuals), were selected as control samples and included in the presented analyses. In each control (**1**, **2** or **3**) the brain tissues revealed different morphologies accordingly to its lateralization and different function based onto four lobes of the brain. That is in agreement with observed differences between human brain's hemispheres, and are explained mostly by the inborn functional asymmetries/lateralization [54,55]. Fig. 1 presents the scanning electron microscopy images of Control 1 brain tissue homogenates from temporal lobe, together with gliomas - Anaplastic Astrocytoma and Glioblastoma on a SERS platforms used during experiments. As can be seen, presented tissue homogenates show different morphologies, even within the Control sample taken from the temporal lobe of the brain (Fig. 1a,b). This is reliable as various cells existing within one brain lobes.

The frontal lobe function is associated with reasoning, motor skills, higher level cognition, and expressive language, the parietal is processing tactile sensory information such as pressure, touch, and pain, the temporal part is responsible for memory, speech perception, and language skills and the occipital function is associated with interpreting visual stimuli and information. The brain cells in lobe dependences contain various patterns and amounts of different cells, e.g. neurons, neuropils, the meshwork of axons, dendrites, synapses and extra cellular matrix of the central nervous system cells, but also glial cells, that constitute the most abundant class of cells in the brain and can generally be subdivided into astrocytes, oligodendrocytes and microglia based on

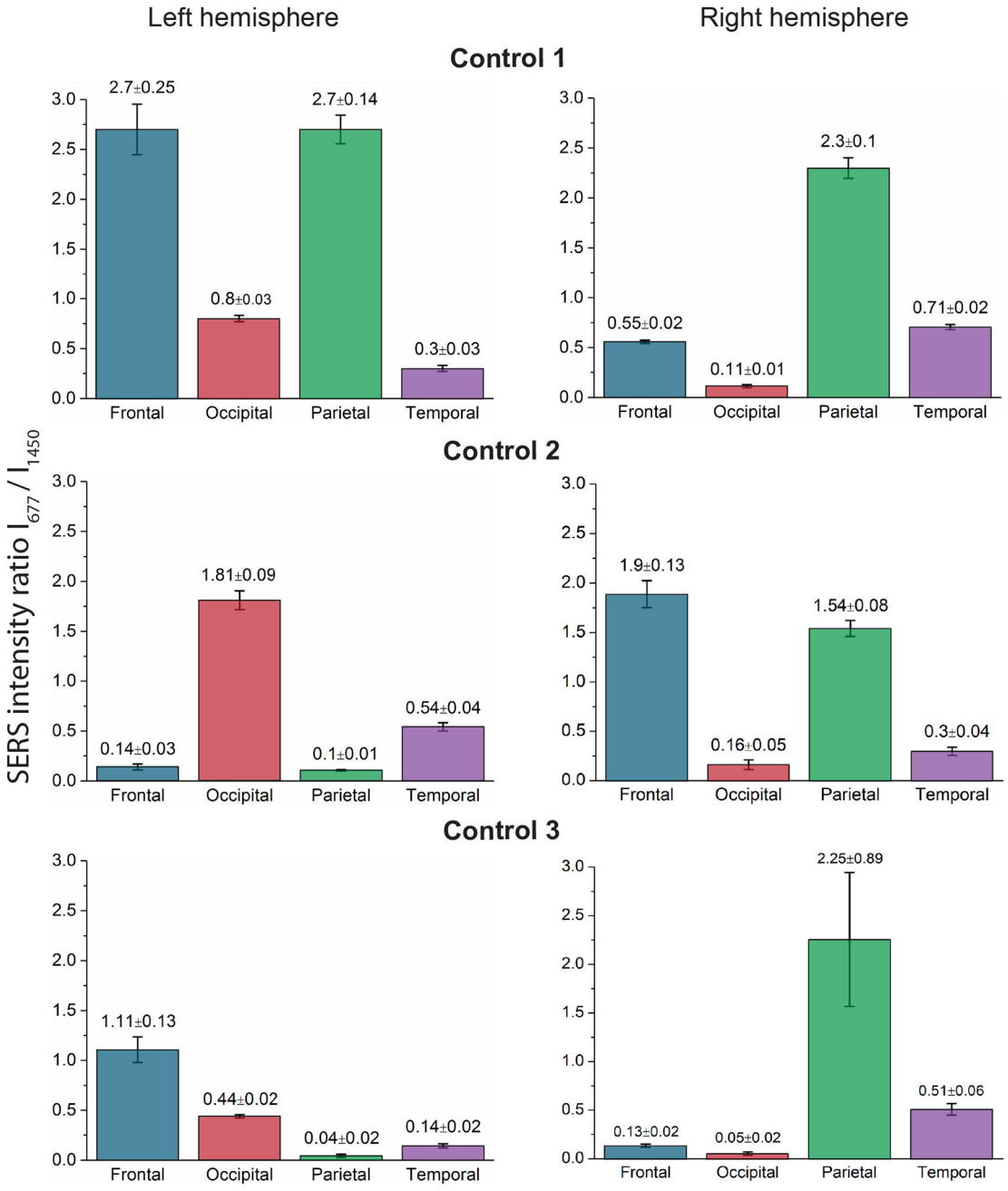

Fig. 3. The SERS intensity plots of I_{677}/I_{1450} vs the brain's part calculated for all controls samples and for both brain's hemispheres, separately. The error bars represent the standard deviation.

morphology and function. Moreover, each brain's hemispheres (left or right) was over last decades considered as differently exploited by particular human and these differences are even more deeper if we consider differences among peoples – diverse logic, linear thinking, intuition, imagination, abilities, talents, behaviour. However, magnetic resonance imaging studies revealed that the human brain doesn't actually favour one side over the other. The networks on one side aren't generally more pronounced than the networks on the other side [56].

Remarkably, SERS spectra presented on Fig. 2a, in dependence on the origin of the control brain homogenates, revealed different spectral features accordingly to its lateralization and different function based onto four different lobes of the brain (see also Fig. S1; Supporting Information). All presented SERS spectra are averages from 20 spectra for one control sample and 40 spectra from one tumour sample of data taken in the mapping mode (Fig. S2 Supporting Information). Observed in Fig. 2a spectral changes are mainly due to different intensities of the revealed bands. Thus, the intensity of the band at 677 cm^{-1}, assigned to vibrations in L-Glutathione and L-Histidine, in comparison to the band intensity at 1450 cm^{-1}, L-Tryptophan vibration, revealed in the spectrum of temporal cells for right brain hemisphere are more higher than its equivalent ratio observed in for left brain hemisphere. For the more examples of this relations, please see Figure S1a,b in Supporting Information. In order to more detailed analysis of the observed spectral changes Fig. 3 presents the bands I_{677}/I_{1450} intensities relationships. Evidently, this relationships are varied in the spectra of both brain hemispheres, as well as for each particular lobes. Thus, it is clear, that variances of the spectral features are closely associated with the tissues origin - the brain lobes. Observed differences in calculated SERS intensities ratio are more pronounced in the spectra of **Control 1** and in right brain's hemisphere, then in two other analysed controls, e.g., **Control 2** and **Control 3** (Fig. 3). The intensities ratio calculated for the left hemisphere in the Occipital and Parietal lobes of Control 1 give approximately the same value, thus as a reference control sample it seems that SERS data collected for **Control 1** and right hemisphere are the most advisable. Besides, that no substantial difference among analysed SERS spectra of control samples are detected.

The SERS spectra of brain tumours homogenates presented on Fig. 2b in comparison to SERS spectra of the control samples (Fig. 2a) show decreasing of tryptophan represented by band at 1450 cm^{-1}. That can be the result of degradation of tryptophan caused by the enzyme indoleamin (2,3)-dioxygenase stimulated by Th1 immune response (IDO) in cancer patients, as it was observed in colorectal [57] and colon [58] tumours. Observed intensity increasing of the band at 1083 cm^{-1} assigned to the nucleic acids, is due to higher nucleic acids bases caused by the abnormal metabolism of DNA and RNA in cancer samples, what is consistent with the data published for cancer patients [51]. The shifts of the band at 1357 cm^{-1} in relation to the SERS of the control sample (band at 1300 cm^{-1}), which are attributed to the nucleic acids, collagen and tryptophan, reveal the importance of these substances changes in the tumour tissues. The same band was observed in the colorectal cancer detected by SERS [59]. Moreover, decreasing of the band at 1629 cm^{-1}; vibration of the porphyrin moiety of hemoglobin; probably indicates that bond breakups have occurred and biofunctions were lost in the occurrence of brain tumour. The assignment of bands observed in the SERS spectra of the control and tumour samples are gathered in Table 1.

All observed changes in the SERS spectral patterns are due to tumour influencing the brain cells. However, those differences show a slight variance in the characteristic spectral features depending on the measurement place, but what is even more important, difference among gathered SERS spectra coming from different tumour samples (Anaplastic Astrocytoma and Glioblastoma cells). Thus they are not sufficient for discrimination purposes and possibility to use them as indicator for tumour detection, what justify including the PCA calculations to the

Table 1
Raman bands assignment observed in spectra of brain control and tumour tissues.

Raman shift (cm^{-1})		
Control	Tumour (**AA, GB**)	Assignment [60]
677	674, 680	L-Glutathione, L-histidine
712	714	CH2 rocking, symmetric breathing, L-tyrosine
753		L-Valine
853		CH2 deformation of tyrosine, proline, glycogen
	879	L-Arginine
803, 874	800	L-Tryptophane
937	937	Guanine
1005		Phenylalanine (ring breathing mode)
	1038	D-(+)-galactosamine
1066	1078, 1083	CC or PO2 stretching, phospholipids in nucleic acids
1129	1125	Adenine
	1183	CC stretching, L-phenylalanine
1252	1261	Thymine, L-tryptophane
1300		Proteins
	1278	Amide III (alfa-helix), L-tryptophane
	1357	Ring breathing of nucleic acids adenine base, CH2CH3 twisting in collagen, tryptophan, L-proline
1453	1450	L-Tryptophan
	1550	Guanine
1585	1586, 1596	L-phenylalanine, L-alanine
1613		CC asymmetric stretching, porphyrin moiety of hemoglobin, L-Serine
1660		Amide *I*, (C═O stretching mode of protein, alfa-helix/random coil; stretching)/C═C lipids stretching

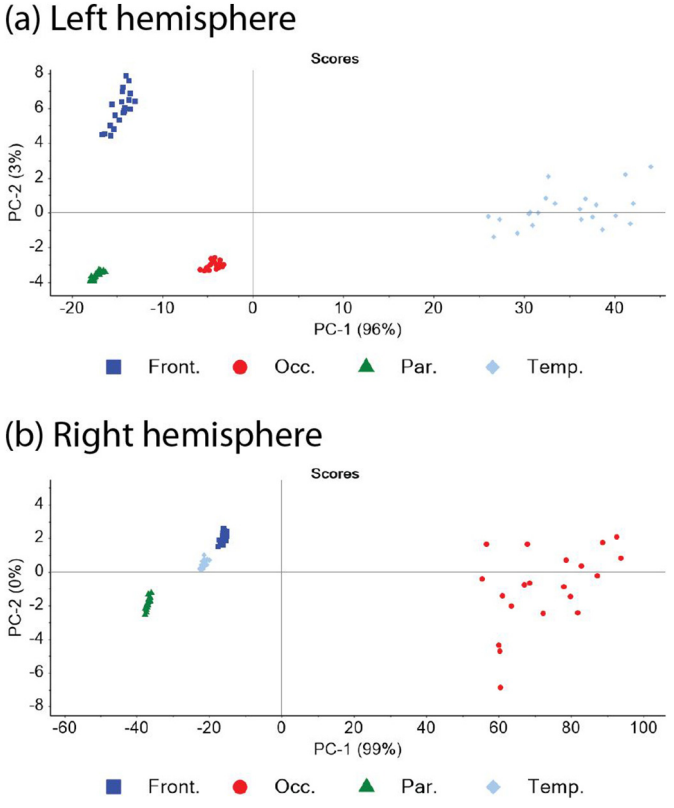

Fig. 4. The plots of PC1 vs. PC2 scores of tissue homogenates, calculated for **Control 1** and four different brain lobes (Front., Par., Temp., Occ. for frontal, temporal, parietal, occipital, respectively) and both left (a) and right (b) brain hemispheres.

Table 2
Explained variances of the first and second PCs calculated for all control, each control and tumour brain together with control samples from data taken for all four parts and right and left side of the brain tissues homogenates separately.

Samples	PC1+ PC2 [%]		
	All	Left	Right
Control (1 + 2 + 3)	91	82	93
Control 1	98	99	99
Control 2	71	75	73
Control 3	89	76	94
Tumours + Control (1 + 2 + 3)	87	73	89
Tumours + Control 1	95	88	96

analysis of the recorded spectra. Thus, with this aim, over the collected SERS spectra the multivariate principal component analysis (PCA) were performed [61]. Firstly, the PCA of control samples were made for three sets of comparisons: (1) all controls together (from both brain's hemispheres), (2) all controls from left hemisphere, (3) all controls from right hemisphere. Results of these calculations, as shown in Fig. 4a,b but also in Fig. S3 (Supporting Information), prove one most important clue – there is always four different groups of PCs scores independently for the left as well as the right parts of brain. Moreover, the observed differences have their direct translation in the obtained PCs values. Furthermore, for the left hemisphere scores of the frontal and the temporal lobes are divided from scores of the occipital and the parietal lobes by PC2 axis (Fig. 4a), as well as, for the right hemisphere by PC2 axis but also by PC1 axis (Fig. 4b). Revealed similarities between the scores of the occipital and the parietal lobes appears for to be more pronounced in the case of data analysed for right hemisphere (Fig. 4b). Observed grouping can be influenced directly by the various morphologies and different function of lobes, what is in good agreement with existing knowledge about human brain's lateralization; different morphologies and different function of each lobes. As is presented on Fig. 4 (data of **1** control) the first main PCs explain 96% of variance for the left hemispheres, while PC1 calculated for the right one explain 99% of total variance among SERS data. It should be highlighted, that similar tendency, the better discrimination among the data collected from the right brain hemisphere, was observed for three considered control samples. These, differences have direct influences onto calculated scores and thus the grouping is more efficient, in all three controls, for the right side of the brain (see Fig. S3 in Supporting Information). Thus, taken into account, that for the **1** control sample and the right side of the brain, the calculated sum of the two main PCs gives 99% of variance, this control were chosen for comparison with the data collected for brain tumour samples. The sum of PC1 and PC2 calculated for all controls are gathered in Table 2.

In the next step the PCA, over the SERS spectra of brain tumour and control samples were utilized to develop diagnostic algorithms for the classification in two associations: (1) all controls and tumours together, (2) each control and tumours. Those analysis were performed for

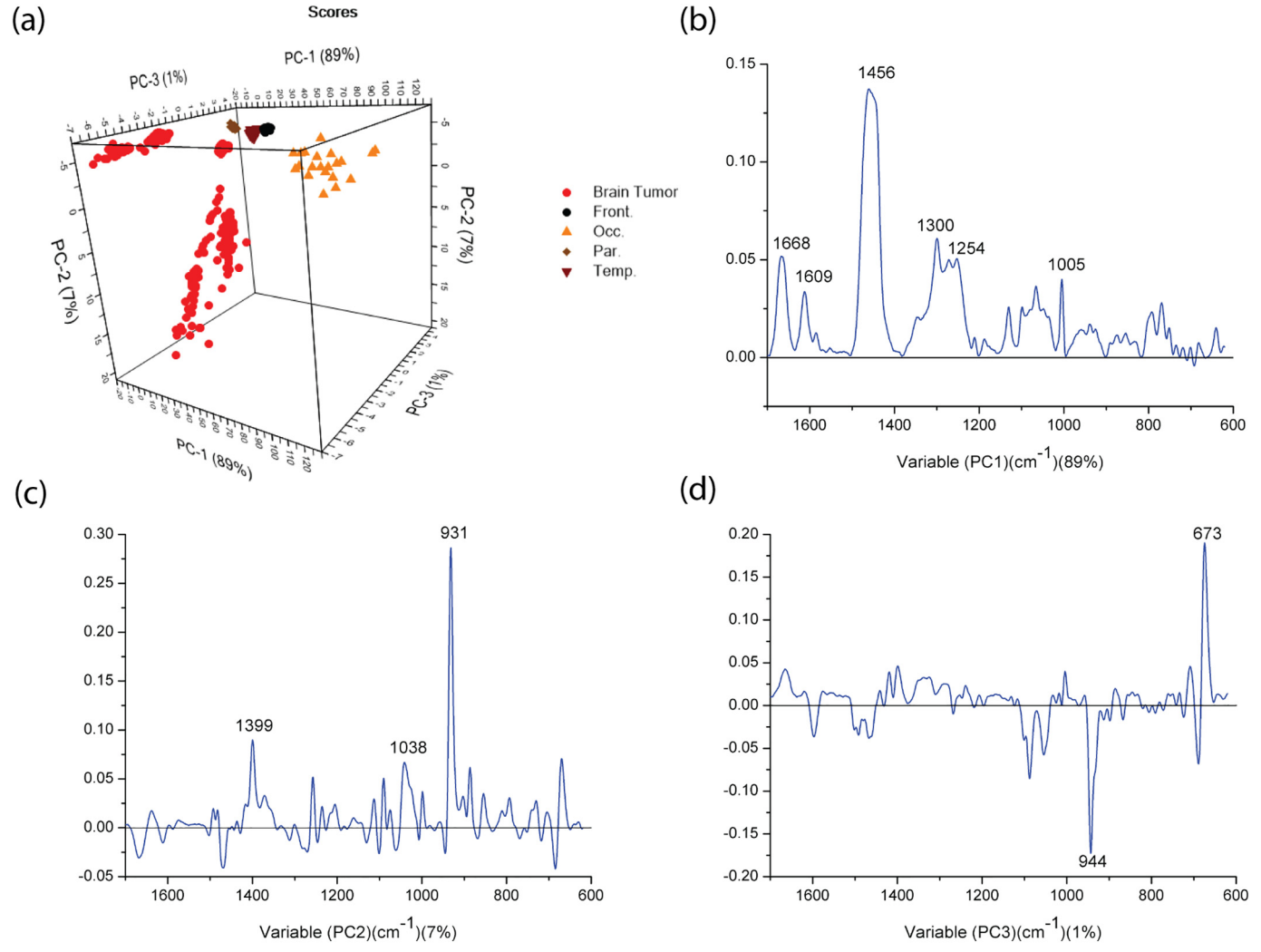

Fig. 5. 3D plots of the PCA scores calculated for homogenates of the brain tumour and **Control 1** group – right brain hemisphere (a) and corresponding loadings data for the PC1 (b), PC2 (c) and PC3 (d).

tumour together with control samples taken out from both brain's hemispheres, and from left and right hemisphere separately. The PCA calculated scores and corresponding loadings data calculated for each the three of the most important PCs, which are enough for discrimination purposes, are presented on Fig. 5 (data brain tumour and Control **1** – right brain hemisphere) and Fig. S4 (for all tumour and controls, as well as tumour with Control **2** and **3**, separately). The all presented scatter plots has the best discrimination performance, e.g. the scores do not overlap. Additionally, the grouping of some scores calculated for the SERS spectra (Anaplastic Astrocytoma and Glioblastoma cells) observed for tumour cells suggests that it can be possible to distinguish each tumour cells based onto PCA calculations. It should be highlighted, that one of the main advantages of the presented method is that the three main PCs describe a total of 96% of the ensemble variance with 89%, 7% and 1% corresponding to the first, second and third PCs, respectively. Thus discrimination among control and tumour brain samples is efficient. The sum of first and second PCs calculated for all controls and chosen one together with brain tumours data performed for all four brain's parts and both hemispheres are presented in Table 2.

For the calculated PCs patterns loadings data reveal the importance of the original SERS variables and indicate the most important variables and regions related to the differences or similarities found in the SERS data set. *Ipso facto* PCA classification allows identification of diagnostic spectral patterns that remain valid for all spectra within a class, even though there may be substantial inter-class variability among spectra. In other words, the loading spectrum of calculated PCs vs. variables (SERS shifts) contains features dependent on differences between the studied groups, i.e. tumour and healthy brain tissues. The weights for each component are represented by a vector called a loadings. The loadings maximize the between-class variance and indicate the variables responsible for diagnostic segregation over the within-class variance (mostly associated with heterogeneity in tissue sample) of the component [62,63].

Loading profiles of the first three PCs calculated for brain tumour and the right hemisphere of the **Control 1** group are displayed in Fig. 5b and for brain tumours and left brain hemisphere of the **Control 1** in Fig. S4b Supporting Information. The bands, which are responsible for the differences between groups in the original SERS spectra can also be found in the loadings spectra, as a most weighted data. The variables at 1005, 1300, 1460 and 1662 cm^{-1} for the loadings plot of PC1 (which accounts for 89% of the total variance), at 670, 932 and 1400 cm^{-1} for PC2 (7%), and at 675, 941 and 1085 cm^{-1} for PC3 (1%) have the highest intensity thus the highest weights for the PCA discrimination of different groups. Therefore, in the loadings dataset, calculated for brain tumour and Control 1 group for the right brain hemisphere (Fig. 5b) and the left hemisphere, separately (Fig. S4b, Supporting Information), the separation is attributed to spectral regions corresponding in SERS spectra to L-Tryptophan (1450, 1278 cm^{-1}), proteins (1300 cm^{-1}), Amide III (1278 cm^{-1}), phenylalanine (1005 cm^{-1}) Amide I (1654 cm^{-1}), Guanine (937 cm^{-1}) (see Table 1).

To summarize, in the scatter plot drawn by PCs, most scores belonging to different groups have little overlap in the PC1-PC2 plot which indicates a good separation between groups. The orthogonal distance plot showed that a good diagnostic accuracy has been obtained by this PCA model. Also, the loadings spectra of PCs enabled us to identify the positions with the highest weights for discriminating groups, and several bonds were found to contribute a large degree to the PC scores. Surprisingly, the calculated scores for the SERS spectra of different tumour cells (Anaplastic Astrocytoma and Glioblastoma cells) are gathered in separated groups. That issues are going to be further explored.

4. Conclusion

Throughout this manuscript we show the potential of the SERS method combined with PCA analysis for discrimination and differentiation between healthy and tumour samples. Firstly, to choose the most proper control for comparison with the data collected for brain tumour samples, the healthy brain tissue samples from both right and left side of the brain's hemispheres for different lobes, e.g., frontal, parietal, temporal and occipital were carefully studied and analysed. As it presented, the first main PCs explain 96% of variance for the left brain hemispheres, while PC1 calculated for the right one explain 99% of total variance among SERS data. That is in good agreement with existing knowledge about human brain's lateralization; different morphologies and different function of each lobes. Then, the PCA over the SERS spectra of brain tumour and control samples were utilized to develop diagnostic algorithms for classification between those samples. The main advantages of the presented method is that the three main PCs describe a total of 96% of the ensemble variance with 89%, 7% and 1% corresponding to the first, second and third PCs, respectively, and indicate the most important variables and regions related to the differences or similarities found in the SERS data set. Such classification allows identification of diagnostic spectral patterns that remain valid for all spectra within a class, even though there may be substantial inter-class variability among spectra. The potential of the proposed method SERS combined with PCA lies mainly in providing differentiation between the control and brain tumours cells what may in future application improves diagnostic accuracy.

Acknowledgments

The Authors would like to thanks Dr. Tomasz Szymborski for SEM images of studied samples. The work was supported by the National Science Centre (Poland) OPUS XIII 2017/25/ST4/01109.

Declaration of competing interest

The authors declare that they have no known competing financial interests or personal relationships that could have appeared to influence the work reported in this paper.

Appendix A. Supplementary data

Supplementary data to this article can be found online at https://doi.org/10.1016/j.saa.2019.117769.

References

[1] P. Khani, F. Nasri, F. Khani Chamani, F. Saeidi, J. Sadri Nahand, A. Tabibkhooei, H. Mirzaei, Genetic and epigenetic contribution to astrocytic gliomas pathogenesis, J. Neurochem. 147 (2018) 0–2, https://doi.org/10.1111/jnc.14616.
[2] American Cancer Society, Survival Rates for Selected Adult Brain and Spinal Cord Tumours, 2015 1. http://www.cancer.org/cancer/braincnstumorsinadults/detailedguide/brain-and-spinal-cord-tumors-in-adults-survival-rates, Accessed date: 22 January 2019.
[3] H. Ohgaki, P. Kleihues, The definition of primary and secondary glioblastoma, Clin. Cancer Res. 19 (2013) 764–772, https://doi.org/10.1158/1078-0432.CCR-12-3002.
[4] P. Wesseling, J.M. Kros, J.W.M. Jeuken, The pathological diagnosis of diffuse gliomas: towards a smart synthesis of microscopic and molecular information in a multidisciplinary context, Diagn. Histopathol. 17 (2011) 486–494, https://doi.org/10.1016/j.mpdhp.2011.08.005.
[5] M. Jermyn, K. Mok, J. Mercier, J. Desroches, J. Pichette, K. Saint-Arnaud, L. Bernstein, M.C. Guiot, K. Petrecca, F. Leblond, Intraoperative brain cancer detection with Raman spectroscopy in humans, Sci. Transl. Med. 7 (2015) 1–10, https://doi.org/10.1126/scitranslmed.aaa2384.
[6] M. Ji, D.A. Orringer, C.W. Freudiger, S. Ramkissoon, X. Liu, D. Lau, A.J. Golby, I. Norton, M. Hayashi, N.Y.R. Agar, G.S. Young, C. Spino, S. Santagata, S. Camelo-Piragua, K.L. Ligon, O. Sagher, X.S. Xie, Rapid, label-free detection of brain tumors with stimulated Raman scattering microscopy, Sci. Transl. Med. 5 (2013) 201ra119, https://doi.org/10.1126/scitranslmed.3005954.
[7] J. Desroches, M. Jermyn, K. Mok, C. Lemieux-Leduc, J. Mercier, K. St-Arnaud, K. Urmey, M.-C. Guiot, E. Marple, K. Petrecca, F. Leblond, Characterization of a Raman spectroscopy probe system for intraoperative brain tissue classification, Biomed. Opt. Express 6 (2015) 2380, https://doi.org/10.1364/BOE.6.002380.
[8] S. Cui, S. Zhang, S. Yue, Raman spectroscopy and imaging for cancer diagnosis, J. Healthc. Eng. 2018 (2018) 1–11, https://doi.org/10.1155/2018/8619342.

[9] J. Zhang, Y. Fan, M. He, X. Ma, Y. Song, M. Liu, J. Xu, Accuracy of Raman spectroscopy in differentiating brain tumor from normal brain tissue, Oncotarget 8 (2017) 36824–36831, https://doi.org/10.18632/oncotarget.15975.

[10] M. Jermyn, J. Desroches, J. Mercier, K. St-Arnaud, M.-C. Guiot, F. Leblond, K. Petrecca, Raman spectroscopy detects distant invasive brain cancer cells centimeters beyond MRI capability in humans, Biomed. Opt. Express 7 (2016) 5129, https://doi.org/10.1364/BOE.7.005129.

[11] S. Nie, S.R. Emory, Probing single molecules and single nanoparticles by surface-enhanced Raman scattering, Author (s): Shuming Nie and Steven R. Emory Published by: American Association for the Advancement of Science Stable URL http://www.jstor.org/stable/2893359.

[12] A. Campion, P. Kambhampati, Surface-enhanced Raman scattering, Chem. Soc. Rev. 27 (1998) 241, https://doi.org/10.1039/a827241z.

[13] C. Zong, M. Xu, L.-J. Xu, T. Wei, X. Ma, X.-S. Zheng, R. Hu, B. Ren, Surface-enhanced Raman spectroscopy for bioanalysis: reliability and challenges, Chem. Rev. 118 (2018) 4946–4980, https://doi.org/10.1021/acs.chemrev.7b00668.

[14] P.L. Stiles, J.A. Dieringer, N.C. Shah, R.P. Van Duyne, Surface-enhanced Raman spectroscopy, Annu. Rev. Anal. Chem. 1 (2008) 601–626, https://doi.org/10.1146/annurev.anchem.1.031207.112814.

[15] J.P. Camden, J.A. Dieringer, Y. Wang, D.J. Masiello, L.D. Marks, G.C. Schatz, R.P. Van Duyne, Probing the structure of single-molecule surface-enhanced Raman scattering hot spots, J. Am. Chem. Soc. 130 (2008) 12616–12617, https://doi.org/10.1021/ja8051427.

[16] X. Gu, M.J. Trujillo, J.E. Olson, J.P. Camden, SERS sensors: recent developments and a generalized classification scheme based on the signal origin, Annu. Rev. Anal. Chem. 11 (2018) 147–169, https://doi.org/10.1146/annurev-anchem-061417-125724.

[17] K. Kneipp, H. Kneipp, V.B. Kartha, R. Manoharan, G. Deinum, I. Itzkan, R.R. Dasari, M.S. Feld, Detection and identification of a single DNA base molecule using surface-enhanced Raman scattering (SERS), Phys. Rev. E Stat. Phys. Plasmas Fluids Relat. Interdiscip. Topics 57 (1998) 3–12, https://doi.org/10.1103/PhysRevE.57.R6281.

[18] R.J. Stokes, E. McBride, C.G. Wilson, J.M. Girkin, W.E. Smith, D. Graham, Surface-enhanced Raman scattering spectroscopy as a sensitive and selective technique for the detection of folic acid in water and human serum, Appl. Spectrosc. 62 (2008) 371–376, https://doi.org/10.1366/000370208784046812.

[19] K. Faulds, W.E. Smith, D. Graham, R.J. Lacey, Assessment of silver and gold substrates for the detection of amphetamine sulfate by surface enhanced Raman scattering (SERS), Analyst 127 (2002) 282–286, https://doi.org/10.1039/b107318b.

[20] A. Sivanesan, E. Witkowska, W. Adamkiewicz, Ł. Dziewit, A. Kamińska, J. Waluk, Nanostructured silver-gold bimetallic SERS substrates for selective identification of bacteria in human blood, Analyst 139 (2014) 1037–1043, https://doi.org/10.1039/c3an01924a.

[21] T.A. Alexander, D.M. Le, Characterization of a commercialized SERS-active substrate and its application to the identification of intact Bacillus endospores, Appl. Opt. 46 (2007) 3878–3890, https://doi.org/10.1364/AO.46.003878.

[22] H.T. Beier, C.B. Cowan, I.H. Chou, J. Pallikal, J.E. Henry, M.E. Benford, J.B. Jackson, T.A. Good, G.L. Coté, Application of surface-enhanced raman spectroscopy for detection of beta amyloid using nanoshells, Plasmonics 2 (2007) 55–64, https://doi.org/10.1007/s11468-007-9027-x.

[23] L.M. Almond, J. Hutchings, G. Lloyd, H. Barr, N. Shepherd, J. Day, O. Stevens, S. Sanders, M. Wadley, N. Stone, C. Kendall, Endoscopic Raman spectroscopy enables objective diagnosis of dysplasia in Barrett's esophagus, Gastrointest. Endosc. 79 (2014) 37–45, https://doi.org/10.1016/J.GIE.2013.05.028.

[24] C.-W. Hsu, C.-C. Huang, J.-H. Sheu, C.-W. Lin, L.-F. Lin, J.-S. Jin, W. Chen, Differentiating gastrointestinal stromal tumors from gastric adenocarcinomas and normal mucosae using confocal Raman microspectroscopy., J. Biomed. Opt. 21 (2016) 75006–1–75006–5. doi:https://doi.org/10.1117/1.JBO.21.7.075006.

[25] C.-W. Hsu, C.-C. Huang, J.-H. Sheu, C.-W. Lin, L.-F. Lin, J.-S. Jin, L.-K. Chau, W. Chen, Novel method for differentiating histological types of gastric adenocarcinoma by using confocal Raman microspectroscopy, PLoS One 11 (2016), e0159829. https://doi.org/10.1371/journal.pone.0159829.

[26] D. Petersen, P. Naveed, A. Ragheb, D. Niedieker, S.F. El-Mashtoly, T. Brechmann, C. Kötting, W.H. Schmiegel, E. Freier, C. Pox, K. Gerwert, Raman fiber-optical method for colon cancer detection: cross-validation and outlier identification approach, Spectrochim. Acta A Mol. Biomol. Spectrosc. 181 (2017) 270–275, https://doi.org/10.1016/j.saa.2017.03.054.

[27] B. Bodanese, L. Silveira, R. Albertini, R.A. Zângaro, M.T.T. Pacheco, Differentiating normal and basal cell carcinoma human skin tissues in vitro using dispersive Raman spectroscopy: a comparison between principal components analysis and simplified biochemical models, Photomed. Laser Surg. 28 (2010) https://doi.org/10.1089/pho.2009.2565119-gniadecka127.

[28] M. Gniadecka, P.A. Philipsen, S. Wessel, R. Gniadecki, H.C. Wulf, S. Sigurdsson, O.F. Nielsen, D.H. Christensen, J. Hercogova, K. Rossen, H.K. Thomsen, L.K. Hansen, Melanoma diagnosis by Raman spectroscopy and neural networks: structure alterations in proteins and lipids in intact cancer tissue, J. Invest. Dermatol. 122 (2004) 443–449, https://doi.org/10.1046/J.0022-202X.2004.22208.X.

[29] B. Bodanese, F.L. Silveira, R.A. Zângaro, M.T.T. Pacheco, C.A. Pasqualucci, L. Silveira, Discrimination of basal cell carcinoma and melanoma from normal skin biopsies *in Vitro* through Raman spectroscopy and principal component analysis, Photomed. Laser Surg. 30 (2012) 381–387, https://doi.org/10.1089/pho.2011.3191.

[30] A. Nijssen, K. Maquelin, L.F. Santos, P.J. Caspers, T.C. Bakker Schut, J.C. den Hollander, M.H.A. Neumann, G.J. Puppels, Discriminating basal cell carcinoma from perilesional skin using high wave-number Raman spectroscopy, J. Biomed. Opt. 12 (2007) 1–7, https://doi.org/10.1117/1.2750287.

[31] T.C. Bakker Schut, P.J. Caspers, G.J. Puppels, A. Nijssen, F. Heule, M.H.A. Neumann, D.P. Hayes, Discriminating basal cell carcinoma from its surrounding tissue by Raman spectroscopy, J. Invest. Dermatol. 119 (2002) 64–69, https://doi.org/10.1046/j.1523-1747.2002.01807.x.

[32] C.J. Frank, R.L. McCreery, D.C.B. Redd, T.S. Gansler, Characterization of human breast biopsy specimens with near-IR Raman spectroscopy, Anal. Chem. 66 (1994) 319–326, https://doi.org/10.1021/ac00075a002.

[33] C.J. Frank, R.L. McCreary, D.C.B. Redd, Raman spectroscopy of normal and diseased human breast tissues, Anal. Chem. 67 (1995) 777–783, https://doi.org/10.1021/ac00101a001.

[34] A.S. Haka, K.E. Shafer-Peltier, M. Fitzmaurice, J. Crowe, R.R. Dasari, M.S. Feld, Diagnosing breast cancer by using Raman spectroscopy, Proc. Natl. Acad. Sci. U. S. A. 102 (2005) 12371–12376, https://doi.org/10.1073/pnas.0501390102.

[35] A.S. Haka, K.E. Shafer-Peltier, M. Fitzmaurice, J. Crowe, R.R. Dasari, M.S. Feld, Identifying microcalcifications in benign and malignant breast lesions by probing differences in their chemical composition using Raman spectroscopy, Cancer Res. 62 (2002) 5375–5380. http://www.ncbi.nlm.nih.gov/pubmed/12235010, Accessed date: 22 January 2019.

[36] N.D. Magee, J.S. Villaumie, E.T. Marple, M. Ennis, J.S. Elborn, J.J. McGarvey, Ex vivo diagnosis of lung cancer using a Raman miniprobe, J. Phys. Chem. B 113 (2009) 8137–8141, https://doi.org/10.1021/jp900379w.

[37] Z. Huang, A. McWilliams, H. Lui, D.I. McLean, S. Lam, H. Zeng, Near-infrared Raman spectroscopy for optical diagnosis of lung cancer, Int. J. Cancer 107 (2003) 1047–1052, https://doi.org/10.1002/ijc.11500.

[38] C. Krafft, B. Belay, N. Bergner, B.F.M. Romeike, R. Reichart, R. Kalff, J. Popp, Advances in optical biopsy-correlation of malignancy and cell density of primary brain tumors using Raman microspectroscopic imaging, Analyst 137 (2012) 5533–5537, https://doi.org/10.1039/c2an36083g.

[39] S. Koljenović, T.C.B. Schut, R. Wolthuis, A.J.P.E. Vincent, G. Hendriks-Hagevi, L. Santos, J.M. Kros, G.J. Puppels, Raman spectroscopic characterization of porcine brain tissue using a single fiber-optic probe, Anal. Chem. 79 (2007) 557–564, https://doi.org/10.1021/ac0616512.

[40] S. Koljenović, L.P. in. Choo-Smith, T.C.B. Schut, J.M. Kros, H.J. Van den Berge, G.J. Puppels, Discriminating vital tumor from necrotic tissue in human glioblastoma tissue samples by Raman spectroscopy, Lab. Investig. 82 (2002) 1265–1277. doi: https://doi.org/10.1097/01.LAB.0000032545.96931.B8.

[41] K. Gajjar, L.D. Heppenstall, W. Pang, K.M. Ashton, J. Trevisan, I.I. Patel, V. Llabjani, H.F. Stringfellow, P.L. Martin-Hirsch, T. Dawson, F.L. Martin, Diagnostic segregation of human brain tumours using Fourier-transform infrared and/or Raman spectroscopy coupled with discriminant analysis, Anal. Methods 5 (2013) 89–102, https://doi.org/10.1039/c2ay25544h.

[42] D. Van de Sompel, E. Garai, C. Zavaleta, S.S. Gambhir, A hybrid least squares and principal component analysis algorithm for Raman spectroscopy, PLoS One 7 (2012), e38850. https://doi.org/10.1371/journal.pone.0038850.

[43] J. Kiefer, Quantitative enantioselective Raman spectroscopy, Analyst 140 (2015) 5012–5018, https://doi.org/10.1039/c5an00878f.

[44] J. Kiefer, K. Noack, Universal enantioselective discrimination by Raman spectroscopy, Analyst 140 (2015) 1787–1790, https://doi.org/10.1039/c4an02218a.

[45] B. Kang, S.S. Li, Q.Y. Guan, A.P. Chen, P.K. Zhang, L. Bin Zhang, J.W. Wei, J.J. Xu, H.Y. Chen, Plasmon-enhanced Raman spectroscopic metrics for in situ quantitative and dynamic assays of cell apoptosis and necrosis, Chem. Sci. 8 (2017) 1243–1250, https://doi.org/10.1039/C6SC02486F.

[46] A. Matschulat, D. Drescher, J. Kneipp, Surface-enhanced Raman scattering hybrid nanoprobe multiplexing and imaging in biological systems, ACS Nano 4 (2010) 3259–3269, https://doi.org/10.1021/nn100280z.

[47] E. Witkowska, D. Korsak, A. Kowalska, M. Księżopolska-Gocalska, J. Niedziółka-Jönsson, E. Roźniecka, W. Michałowicz, P. Albrycht, M. Podrażka, R. Hołyst, J. Waluk, A. Kamińska, Surface-enhanced Raman spectroscopy introduced into the international standard organization (ISO) regulations as an alternative method for detection and identification of pathogens in the food industry, Anal. Bioanal. Chem. 409 (2017) 1555–1567, https://doi.org/10.1007/s00216-016-0090-z.

[48] Z. Shi, C.E. Castro, G. Arya, Conformational dynamics of mechanically compliant DNA nanostructures from coarse-grained molecular dynamics simulations, ACS Nano 11 (2017) 4617–4630, https://doi.org/10.1021/acsnano.7b00242.

[49] M. Fernandez, A.S. Barnard, Identification of nanoparticle prototypes and archetypes, ACS Nano 9 (2015) 11980–11992, https://doi.org/10.1021/acsnano.5b05788.

[50] M. Fernandez, H.F. Wilson, A.S. Barnard, Impact of distributions on the archetypes and prototypes in heterogeneous nanoparticle ensembles, Nanoscale 9 (2017) 832–843, https://doi.org/10.1039/C6NR07102C.

[51] R.Y. Sato-Berrú, E.V. Mejía-Uriarte, C. Frausto-Reyes, M. Villagrán-Muniz, J.M. Saniger, Application of principal component analysis and Raman spectroscopy in the analysis of polycrystalline BaTiO3at high pressure, Spectrochim. Acta A Mol. Biomol. Spectrosc. 66 (2007) 557–560, https://doi.org/10.1016/j.saa.2006.03.032.

[52] R. Bro, A.K. Smilde, Principal component analysis, Anal. Methods 6 (2014) 2812–2831, https://doi.org/10.1039/C3AY41907J.

[53] K. Niciński, E. Witkowska, D. Korsak, K. Noworyta, J. Trzcińska-Danielewicz, A. Girstun, A. Kamińska, Photovoltaic cells as a highly efficient system for biomedical and electrochemical surface-enhanced Raman spectroscopy analysis, RSC Adv. 9 (2019) 576–591, https://doi.org/10.1039/C8RA08319C.

[54] M.C. Corballis, Left brain, right brain:facts and fantasies, PLoS Biol. 12 (2014) 1–6, https://doi.org/10.1371/journal.pbio.1001767.

[55] S.J. Gotts, H.J. Jo, G.L. Wallace, Z.S. Saad, R.W. Cox, A. Martin, Two distinct forms of functional lateralization in the human brain, Proc. Natl. Acad. Sci. 110 (2013) E3435–E3444, https://doi.org/10.1073/pnas.1302581110.

[56] J.A. Nielsen, B.A. Zielinski, M.A. Ferguson, J.E. Lainhart, J.S. Anderson, An evaluation of the left-brain vs. right-brain hypothesis with resting state functional connectivity magnetic resonance imaging, PLoS One 8 (2013) 1, https://doi.org/10.1371/journal.pone.0071275.

[57] A. Huang, D. Fuchs, B. Widner, C. Glover, D.C. Henderson, T.G. Allen-Mersh, Serum tryptophan decrease correlates with immune activation and impaired quality of life in colorectal cancer, Br. J. Cancer 86 (2002) 1691–1696, https://doi.org/10.1038/sj.bjc.6600336.

[58] X. Li, T. Yang, S. Li, D. Wang, Y. Song, S. Zhang, Raman spectroscopy combined with principal component analysis and k nearest neighbour analysis for non-invasive detection of colon cancer, Laser Phys. 26 (2016) 1–9, https://doi.org/10.1088/1054-660X/26/3/035702.

[59] L. Duo, F. Shangyuan, P. Jianji, C. Yanping, L. Juqiang, C. Guannan, X. Shusen, Z. Haishan, C. Rong, Colorectal cancer detection by gold nanoparticle based surface-enhanced Raman spectroscopy of blood serum and statistical analysis, Opt. Express 19 (2011) 13565–13577, https://doi.org/10.1364/oe.19.013565.

[60] L.M. Joke De Gelder, Kris De Gussem, Peter Vandenabeele, Reference database of Raman spectra of biological molecules, J. Pure Appl. Microbiol. 38 (2007) 1133–1147, https://doi.org/10.1002/jrs.

[61] PCA can be described as uncorrelated linear combination of the original variables (X) as X = t1p′1 + t2p′2 +…2 + tAp′A + E = TP + E, where A is the total number of extracted PCs, t (scores) and p (loadings) are the new latent variables and E is the resi, (n.d.) PCA can be described as uncorrelated linear combin.

[62] V. Llabjani, J. Trevisan, K.C. Jones, R.F. Shore, F.L. Martin, Derivation by infrared spectroscopy with multivariate analysis of bimodal contaminant-induced dose-response effects in MCF-7 cells, Environ. Sci. Technol. 45 (2011) 6129–6135, https://doi.org/10.1021/es200383a.

[63] J.F. Trevor Hastie, R. Tibshirani, The elements of statistical learning, Data Mining, Inference and Prediction, Springer-Verlag, New York, New York, 2009https://doi.org/10.1007/978-0-387-84858-7.